AGU PUBLICATIONS

JGR

Journal of Geophysical Research: Atmospheres

RESEARCH ARTICLE
10.1002/2014JD021794

Key Points:
- Hydroperoxyl radical levels were similar at TMS and at TW
- HO_x production was dominated by O_3 photolysis at TMS
- O_3 destruction was ruled by $OH + NO_2$ reaction at TW

Supporting Information:
- Readme
- Tables S1–S6

Correspondence to:
H. Guo,
ceguohai@polyu.edu.hk

Citation:
Ling, Z. H., H. Guo, S. H. M. Lam, S. M. Saunders, and T. Wang (2014), Atmospheric photochemical reactivity and ozone production at two sites in Hong Kong: Application of a Master Chemical Mechanism–photochemical box model, *J. Geophys. Res. Atmos.*, *119*, 10,567–10,582, doi:10.1002/2014JD021794.

Received 27 MAR 2014
Accepted 20 AUG 2014
Accepted article online 23 AUG 2014
Published online 11 SEP 2014

Atmospheric photochemical reactivity and ozone production at two sites in Hong Kong: Application of a Master Chemical Mechanism–photochemical box model

Z. H. Ling[1,2], H. Guo[2], S. H. M. Lam[3], S. M. Saunders[3], and T. Wang[2]

[1]School of Environmental Science and Engineering, Sun Yat-Sen University, Guangzhou, China, [2]Air Quality Studies, Department of Civil and Environmental Engineering, Hong Kong Polytechnic University, Hong Kong, China, [3]School of Chemistry and Biochemistry, University of Western Australia, Perth, Western Australia, Australia

Abstract A photochemical box model incorporating the Master Chemical Mechanism (v3.2), constrained with a full suite of measurements, was developed to investigate the photochemical reactivity of volatile organic compounds at a semirural site (Mount Tai Mo Shan (TMS)) and an urban site (Tsuen Wan (TW)) in Hong Kong. The levels of ozone (O_3) and its precursors, and the magnitudes of the reactivity of O_3 precursors, revealed significant differences in the photochemistry at the two sites. Simulated peak hydroperoxyl radical (HO_2) mixing ratios were similar at TW and TMS ($p = 0.05$), while the simulated hydroxyl radical (OH) mixing ratios were much higher at TW ($p < 0.05$), suggesting different cycling processes between OH and HO_2 at the two sites. The higher OH at TW was due to high-NO mixing ratios, which shifted the HO_x ($OH + HO_2$) balance toward OH by the propagation of HO_2 and alkyl peroxy radicals (RO_2) with NO. HO_x production was dominated by O_3 photolysis at TMS, but at TW, both HCHO and O_3 photolyses were found to be major contributors. By contrast, radical-radical reactions governed HO_x radical losses at TMS, while at TW, the $OH + NO_2$ reaction was found to dominate in the morning and the radical-radical reactions at noon. Overall, the conversion of NO to NO_2 by HO_2 dictated the O_3 production at the two sites, while O_3 destruction was dominated by the $OH + NO_2$ reaction at TW, and at TMS, O_3 photolysis and the $O_3 + HO_2$ reaction were the major mechanisms. The longer OH chain length at TMS indicated that more O_3 was produced for each radical that was generated at this site.

1. Introduction

It is well recognized that high ozone (O_3) concentrations have detrimental effects on human health, crops, and vegetation, in addition to its central roles in photochemistry and the oxidizing capacity in the lower atmosphere [*National Research Council*, 1991; *Seinfeld and Pandis*, 2006]. The O_3 abundance in the atmosphere is determined by downward transport from the stratosphere, dry deposition to the Earth's surface, and the in situhotochemical formation through reactions involving volatile organic compounds (VOCs) and nitrogen oxides (NO_x) in the presence of sunlight [*Jenkin and Clemitshaw*, 2000; *Seinfeld and Pandis*, 2006].

The mechanisms of photochemical reactions resulting in O_3 formation have been studied for decades. The hydroxyl radical (OH), primarily formed via O_3 photolysis, predominantly initiates the reaction sequence. The OH radical reacts with both saturated and unsaturated VOCs to produce alkyl peroxy radicals (RO_2) and hydroperoxyl radicals (HO_2), which convert NO to NO_2 efficiently. Among these reactions, the formation of RO_2 is the rate-controlling step [*Gilman et al.*, 2009]. Finally, NO_2 is converted back to NO by photolysis, resulting in the regeneration of O_3. The photochemical O_3 formation has a nonlinear relationship with its precursors, i.e., VOC- or NO_x-sensitive chemistry, which is dependent on the relative concentrations of NO_x and VOCs [*Sillman*, 1999; *Jenkin and Clemitshaw*, 2000; *Lu et al.*, 2010; *Liu et al.*, 2012]. At low [VOC]/[NO_x] ratios (i.e., a VOC-sensitive regime), the reaction between OH and NO_2 is the dominant chain-terminating reaction, competing with chain-propagating reactions of OH and VOCs. Therefore, reducing the concentration of VOC would theoretically lead to a decrease in O_3 formation. On the other hand, at high [VOC]/[NO_x] ratios (i.e., a NO_x-sensitive regime), the peroxy-peroxy reactions are the dominant chain-terminating reactions, while the oxidation of NO to NO_2 by hydroperoxyl and alkyl peroxy radicals is the key propagating

reaction, which subsequently forms O_3. Hence, in theory, any reduction in NO_x would decrease the photochemical O_3 formation. However, the boundaries between these regimes are not fixed, and there is also the condition in transition between the two cases, making control of photochemical O_3 complex and difficult.

The most urbanized and industrialized region in southern China, the Pearl River Delta (PRD) including Hong Kong, is experiencing severe O_3 pollution with the hourly mixing ratio frequently exceeding 100 ppbv in recent years due to large local emissions of its precursors and long-range transport from eastern China [*Wang et al.*, 2009; *Zheng et al.*, 2010; *HKEPD (Hong Kong Protection Department)*, 2012a; *Ling et al.*, 2013]. Although many studies have investigated the O_3 pollution in this region, most focused on the spatiotemporal variations, the influence of meteorological conditions, and the NO_x- and/or VOC-limited regimes for the photochemical O_3 formation [*Zhang et al.*, 2007, 2008; *Jiang et al.*, 2008, 2010; *Cheng et al.*, 2010; *Ling et al.*, 2011; *Guo et al.*, 2009, 2013; *Wang et al.*, 2006, 2009]. For example, it has been reported that the outflow of polluted continental air and the inflow of maritime air helped shape the seasonal patterns of O_3 in Hong Kong [*Chan et al.*, 1998a, 1998b]. Regional transport has been shown to have significant influence on the redistribution of air pollutants between inland PRD and Hong Kong, based on the results of ratio analyses and Lagrangian trajectories and dispersion simulation [*Guo et al.*, 2009]. With the same data set, a comparison of meteorological conditions between O_3 and non-O_3 episode days confirmed that higher temperature, stronger solar radiation, lower relative humidity, lower wind speed, and northerly winds could induce high O_3 levels observed in the PRD region [*Cheng et al.*, 2010]. In addition, observation-based model studies [*Zhang et al.*, 2007; *Cheng et al.*, 2010] showed that between 50 and 100% of the observed high O_3 in Hong Kong during O_3 episode days were attributed to local photochemical generation and that the O_3 formation was generally VOC-limited.

In contrast, limited studies have been conducted to understand in detail the drivers controlling the chemical mechanisms of O_3 formation in this region. One important study in the region was the extensive field campaign conducted at a downwind site in the inland PRD region in July 2006 [*Hofzumahaus et al.*, 2009; *Lou et al.*, 2010; *Lu et al.*, 2012, 2014, and related papers], which discovered high OH concentrations ($15–26 \times 10^6$ cm^{-3}) with a large OH reactivity of about 20 s^{-1} at noon in a VOC-rich atmosphere in inland PRD. However, the levels of O_3 and its precursors and the meteorological conditions in Hong Kong are significantly different from those in the inland PRD, although they are neighbors [*AFCD (Agriculture, Fisheries and Conservation Department)*, 2008; *Guo et al.*, 2009; *Louie et al.*, 2012; *Zhong et al.*, 2013; *Guo et al.*, 2014]. Hence, it is crucial to gain a better understanding of the photochemistry of O_3 and its precursors in Hong Kong.

Moreover, most of the previous studies were undertaken at low-elevation urban, suburban, and rural sites. There is little knowledge about the variations of O_3 and its precursors and related photochemical reactivity at different elevations in the mountainous areas in this region, where topography and physical features are complex and severe O_3 pollution has been observed for decades. Hence, concurrent measurements were conducted at different elevations of the highest mountain in Hong Kong in autumn for the first time. The autumn field campaign during the typical period of photochemical pollution was commonly observed in Hong Kong and/or the inland PRD region in order to investigate the characteristics of photochemical air pollutants and the factors that impact O_3 variations at different elevations in this mountainous area of Hong Kong [*Guo et al.*, 2013]. A photochemical box model coupled with the Master Chemical Mechanism (PBM-MCM) was developed for the first time based on the measured data to understand the detailed chemistry involved in O_3 formation under the influence of different levels of O_3 precursors at the two sites in Hong Kong [*Lam et al.*, 2013]. Compared to the previous study, this study extends the modeling to further investigate the variations of HO_x and its sources and sinks, the contributions of different pathways to O_3 production and destruction, and the O_3 production efficiency related to OH regeneration. The data presented are valuable for improving current understanding of O_3 pollution and its related photochemistry in the complex topography of Hong Kong. The study is beneficial for understanding photochemical pollution at an elevated mountain site and serves as a complement to previous studies conducted in low-elevation areas of Hong Kong and the PRD.

Simultaneous field measurements were conducted at a semirural site (i.e., Mount Tai Mo Shan (TMS)) and an urban site (i.e., Tsuen Wan (TW)) in Hong Kong from 6 September to 29 November. An overview of the project has been reported previously [*Guo et al.*, 2013], which included both non-O_3 and O_3 episode days between 28 September and 21 November 2010, with an O_3 episode day defined when the 1 h O_3 mixing ratio is above

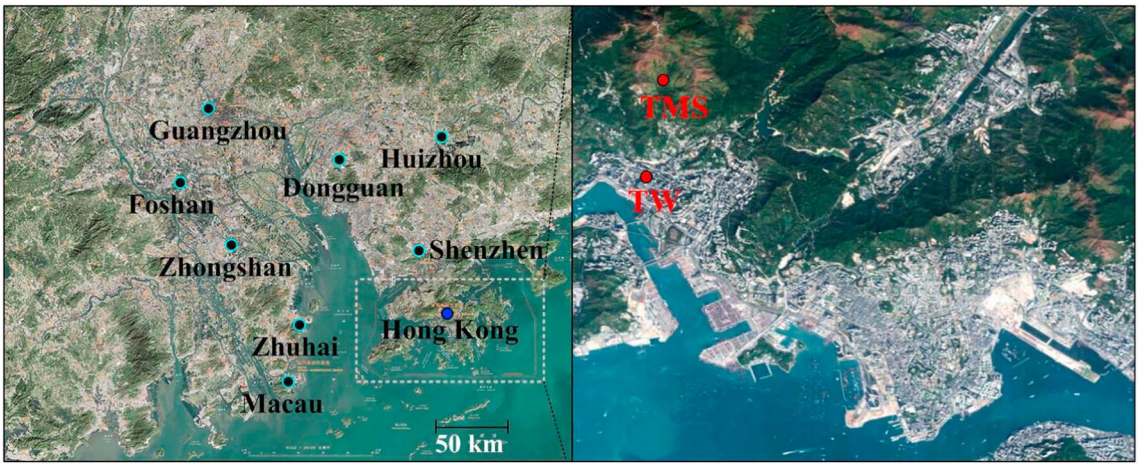

Figure 1. Sampling locations of the semirural mountain site at Tai Mo Shan (TMS) and urban site at Tsuen Wan (TW) in Hong Kong, shown in relation to the Pearl River Delta (PRD) region.

100 ppbv (i.e., China's Grade II Standard). In this study, we mainly focused on a period of time, when there were large variations of O_3 and its precursors at the two sites and the field measurements were intensive. The aims were to investigate the differences in O_3 photochemistry at the two sites when concurrently different relative concentrations of O_3 and its precursors were observed. The findings would provide valuable insight for the alleviation of the O_3 pollution in Hong Kong, a part of the PRD region that experiences frequent severe O_3 events. We first studied the variations of O_3 and its precursors at the two sites in an "O_3 episode" period, i.e., from 27 October to 03 November 2010, when large O_3 variations and elevated O_3 mixing ratios were found at the TMS and TW locations. During the above period, O_3 mixing ratios increased and stayed at high levels (~100 ppbv) at TMS while remained low at TW. We then evaluated the changes in photochemical reactivity at the two sites with different levels of O_3 and its precursors by using the newly developed PBM-MCM [*Lam et al.*, 2013], constrained with a full suite of measurement data, i.e., meteorological conditions, VOCs, and trace gases, i.e., SO_2, CO, and NO_x. Briefly, the chemical mechanisms for the input reactants, the boundary layer conditions, and the abundance and photolysis rates of particular VOCs were revised to meet the actual conditions in the PRD region. It is noteworthy that this is the first study on the investigation of the detail of photochemical reactivity in subtropical Hong Kong and southern China using such a chemically explicit model. The identified target issues addressed in this study were (1) what was the difference in photochemical oxidation between the two sites? and (2) what were the roles of photochemical oxidation in the in situ photochemical O_3 formation at the two sites?

2. Methodology

2.1. Site Description and Instrumentation

The field campaign was conducted at two different elevations of the highest mountain in Hong Kong (elevation = 967 m), i.e., Mount Tai Mo Shan (Mount TMS). Mount TMS, located in the New Territories of Hong Kong, is surrounded by 1440 ha of natural territory with Country Parks to the east, south, and west. Surrounding the foot of the mountain are urban centers with a population of 2.23 million, with Tsuen Wan to the south, Sha Tin to the east, Tuen Mum to the west, and Yuen Long to the north. Farther to the south and southwest is the South China Sea, and to the north is the inland PRD region. Figure 1 shows the two sampling locations and the surroundings. In this study, one sampling site, i.e., TMS, was set on the rooftop of a building at the elevation of 640 m, being the highest possible observation location, beyond which to the mountain summit is only natural territory with shrubs and grasses [*AFCD (Agriculture, Fisheries and Conservation Department)*, 2008] (Figure 1). Another site, i.e., the urban site at the foot of the mountain, was the monitoring station of the Hong Kong Environmental Protection Department (HKEPD) at Tsuen Wan (TW), classified as a mixed residential, commercial, and light industrial area [*Guo et al.*, 2004]. The linear distance between the two sites was about 7 km, and the difference in elevation between the two sites was 630 m. Due to its unique topography, mesoscale circulations, i.e., mountain-valley and sea-land breezes, are frequently observed in the study area, which could influence the redistribution of air pollutants between the two sites [*Guo et al.*, 2013].

In addition to the mesoscale circulations, the average height of boundary layer in the study area during the sampling period, estimated to range from $<$500 m to $>$1500 m based on the results of previous studies [*He et al.*, 2008; *Yang et al.*, 2013], could have influence on the variations of air pollutants at the two sites [*Guo et al.*, 2012]. Trace gas data including O_3, CO, NO-NO_2-NO_x, and SO_2 were collected continuously at TMS. The O_3 was measured using a commercial UV photometrix analyzer (Advanced Pollution Instrumentation (API), model 400E) and CO by a gas filter correlation, nondispersive infrared analyzer (API, model 300E). Nitrogen oxides were detected by a commercial chemiluminescence NO-NO_2-NO_x analyzer with an internal molybdenum converter (API, model 200E), and SO_2 was analyzed with a pulsed UV fluorescence monitor (API, model 100E). Meteorological parameters, i.e., temperature, relative humidity, wind speed and wind direction, and solar radiation, were collected by a weather station (Vantage Pro2 Plus^{TM} Weather Station, Davis Instruments) and averaged to hourly data. The detection limits and quality assurance and control protocols of the trace gas analyzers are provided in detail in the previous report [*Guo et al.*, 2013].

At TW, the hourly data of the above trace gases and meteorological parameters were obtained from the HKEPD monitoring station (http://epic.epd.gov.hk/ca/uid/airdata). The trace gas analyzers used at TW were the same as those at the TMS site, while the meteorological parameters were collected by an automatic weather station (M.R. Young, USA). Further information about the measurements, quality assurance, and control protocols at the TW site can be found in the HKEPD report [*HKEPD (Hong Kong Protection Department)*, 2012b].

2.2. Sampling and Analysis of VOCs

Concurrent VOC canister and carbonyl cartridge samples were collected on 10 O_3 episode days and 10 non-O_3 episode days at TMS and TW, respectively. The O_3 episode days, as given in the introduction, were defined based on the O_3 mixing ratios at TMS with maximum hourly average concentrations exceeding 100 ppbv. Before sampling, the potentially high-O_3 episode days were forecasted based on meteorological conditions and weather prediction. Stronger solar radiation, lower wind speeds, and less vertical dilution of air pollution were usually found on high-O_3 episode days compared to non-O_3 episode days. The potential O_3 episode days forecasted were later confirmed by the observed O_3 mixing ratios. In this study, the non-O_3 episode days included 28 September; 2, 8, 14, 18,19, 27, and 28 October; and 21 and 22 November 2010, while the O_3 episode days were 23, 24, and 29–31 October and 1–3, 9, and 19 November 2010.

Ambient VOC samples were collected using cleaned and evacuated 2 L electropolished stainless steel canisters, which were prepared and delivered by the Rowland/Blake group at the University of California, Irvine, before the sampling campaign. A flow-controlling device was used to collect 1 h integrated samples. During non-O_3 episode days, the 1 h samples were collected with a frequency of 2 h between 07:00 and 19:00 local time (LT). On O_3 episode days, 1 h samples were consecutively taken each hour from 09:00 to 16:00 LT with additional samples collected at 18:00, 21:00, 00:00, 03:00, and 07:00 LT, respectively. Detailed information of the analysis system and quality control and quality assurance for VOC samples are reported elsewhere [*Simpson et al.*, 2010]. In total, 54 nonmethane hydrocarbons (NMHCs), oxygenated VOCs (OVOCs), and methane were determined in this study. The detection limit of aromatics was 3 parts per trillion by volume (pptv), while that of other VOCs was 5 pptv. The accuracy of the measurements was 5%, whereas the measurement precision was 0.5–16% [*Simpson et al.*, 2010].

In addition to VOC samples, 2 h carbonyl samples were concurrently collected between 07:00 and 19:00 LT at both sites during non-O_3 episode days with additional samples at 00:00 and 03:00 LT during O_3 episode days. C_1–C_8 carbonyl compounds were measured by high-performance liquid chromatography with the detection limit of 0.2 ppbv, while the relative percent differences for duplicate analysis were within 10%. Further information is reported in an earlier study [*Guo et al.*, 2009].

2.3. Model Description and Configurations

A photochemical box model coupled with the Master Chemical Mechanism (PBM-MCM) was used to simulate the photochemistry of O_3 formation, free radicals, and intermediate products at the two different locations in Hong Kong for selected O_3 episode days of the field campaign period. The MCM used in this study (version 3.2; University of Leeds website, http://mcm.leeds.ac.uk/MCM/) is a state-of-the-art chemical mechanism, which describes the oxidation of 143 VOCs including methane and contains around 16,500 reactions involving 5900 chemical species [*Jenkin et al.*, 1997b, 2003; *Saunders et al.*, 2003]. Simulations were carried

out for the O_3 episode period from 27 October to 3 November 2010. The measured parameters, including O_3, CO, NO_x, SO_2, 54 VOCs, and methane, temperature, pressure, and relative humidity were used as input. The model was further tailored for the actual conditions in the region including the boundary layer and photolysis rates of particular VOCs [*Lam et al.*, 2013]. The model output simulated O_3 formation as well as the full set of precursors, radicals, and intermediates. A complete description of the model construct has been reported previously [*Lam et al.*, 2013]. In brief, the PBM-MCM was developed based on the assumptions that the PBM was a well-mixed box without treatment of vertical or horizontal dispersion and the air pollutants in this model were homogeneous. In addition, the MCM used in this study defined only the details of the photochemical reactions, in terms of species and reaction rates, which would not change from model to model application, apart from the calculated photolysis rate. Therefore, to provide robust simulation results for the photochemical reactivity in this study, several measures were adopted to control the accuracy for the model simulation. First, the model used was the latest version of Master Chemical Mechanism (MCMv3.2). The MCM chemistry framework has been tested and validated over a wide range of conditions, which have been presented in numerous studies [e.g., *Jenkin et al.*, 1997a, 2003; *Carslaw et al.*, 1999; *Altenstedt and Pleijel*, 2000; *Derwent et al.*, 1998a, 1998b, 2003, 2007, 2010; *Emmerson et al.*, 2005; *Evtyugina et al.*, 2007; *Pinho et al.*, 2009; *Sommariva et al.*, 2008, 2011; *Utembe et al.*, 2005; *Walker et al.*, 2009] and compared with other available mechanisms [*Derwent and Murrells*, 2013a, 2013b]. In addition, due to the fact that neither $J(O^1D)$ nor $J(NO_2)$ used in the previous studies [*Carslaw et al.*, 2001; *Hofzumahaus et al.*, 2009, and related papers] was measured as part of this study, the photolysis rates of different species in this study were parameterized according to the approach of previous work [*Pinho et al.*, 2009] using the photon flux determined from the Tropospheric Ultraviolet and Visible Radiation (v5) model based on the actual conditions, i.e., meteorological parameters, location, and time period of the field campaign in Hong Kong. The modeled OH concentration profiles presented good correspondence with the only available direct field measurements of OH in the region to date, which aimed to quantify the OH concentration and related photochemical reactivity based on field measurements conducted in a semirural vegetated region northwest of Guangzhou City in the PRD region in 2006 [*Hofzumahaus et al.*, 2009, and related papers]. Although the modeled results in this study were relatively lower than those observed in the field campaign of 2006, due to the differences in the levels of O_3 and its precursors, and to a lesser extent, meteorological conditions, the updated photolysis parameterization gave a significantly improved representation of the OH diurnal profile compared to the earlier MCM photolysis parameterization [*Lam et al.*, 2013], suggesting that the model simulation for the photochemical reactivity was appropriate at TMS and TW in this study. Furthermore, the model was constrained with direct measurement data from the field campaign. The key differences in the model setup were in the actual VOC, NO_x, trace gases, and meteorological conditions measured, which drove the differences in the photochemical reactivity simulated at the two sites. In addition, for the variations of O_3, the results indicated that the model simulated well the peak and the diurnal patterns of O_3 during the study period [*Lam et al.*, 2013], further confirming that the photochemical box model used in this study could provide a reasonable description of O_3 formation and related photochemical reactivity at TMS and TW.

3. Results and Discussion

3.1. Characteristics of Air Pollutants During the Episode Event

3.1.1. Overview of O_3 and Its Precursors

The variations in the O_3 measurements have been overviewed previously [*Guo et al.*, 2013]. In general, the mixing ratios of O_3 were higher at TMS than at TW, which could be related to the combined effects of NO titration, vertical meteorological conditions, regional transport, and mesoscale circulations. In the present study, the average mixing ratios of O_3 were 35 ± 2 and 73 ± 3 ppbv for TW and TMS, respectively. In addition, 6 days, i.e., from 29 October to 03 November, were classified as O_3 episode days at TMS, with daytime maximum values higher than 100 ppbv (i.e., China's Grade II Standard), while the daytime maximum mixing ratios of O_3 at TW were within the range of 48~66 ppbv for the same period. Apart from O_3, Table 1 presents the median, average, and maximum mixing ratios of 55 VOCs (including methane) together with CO and NO_2 at TMS and TW during the O_3 episode event. Most of the compounds in Table 1 are primarily categorized by chemical class, while some species are grouped by their sources, e.g., isoprene and terpenes classified as biogenic VOCs (BVOCs). In general, the mixing ratios of VOCs were higher at TW than at TMS due to the difference of sampling locations, with the average total VOC concentrations of 42 ± 2 (mean $\pm$ 95% confidence interval) and 25 ± 1 ppbv, respectively. At TMS, oxygenated VOCs (OVOCs) dominated the total

Table 1. Descriptive Statistics of the Mixing Ratios of Measured Compounds at TMS and TW and Their OH Reaction Rate Coefficients

	TMS (pptv)			TW (pptv)			
Compound	Median	Average	Maximum	Median	Average	Maximum	k_{OH}[a]
			Alkanes				
Ethane	1971	2015	2590	2250	2299	3446	0.25
Propane	1022	1037	2560	2598	3027	10427	1.1
n-butane	626	672	2983	3065	3834	16121	2.4
i-butane	473	540	3174	1887	2327	8279	2.1
n-pentane	221	403	4507	340	408	2056	3.8
i-pentane	319	430	2886	489	627	4942	3.6
n-hexane	157	190	756	211	308	1457	5.2
2-methylpentane	129	157	667	194	228	2045	5.6
3-methylpentane	90	108	361	124	145	1136	5.2
n-heptane	81	95	290	134	168	1335	6.8
n-octane	25	29	84	42	52	751	8.1
n-nonane	23	29	81	52	57	413	9.7
n-decane	26	31	107	58	62	133	11
			Alkenes				
Ethene	675	715	1816	1526	1715	5936	8.5
Propene	92	120	510	387	464	2555	26.3
1-butene	27	33	122	64	72	216	31.4
i-butene	84	221	3591	175	285	1465	51.4
Trans-2-butene	3	6	40	22	28	242	64
cis-2-butene	4	5	26	17	22	204	56.4
1,3-butadiene	2	4	54	39	43	157	66.6
1-pentene	13	17	97	24	34	279	31.4
Ethyne	1638	1621	2541	2557	2552	4366	0.9
			Aromatics				
Benzene	614	640	1022	752	739	1195	1.2
Toluene	1428	1729	6079	2830	2187	23919	5.6
Ethylbenzene	307	439	1591	459	585	2201	7.0
m-xylene	137	210	1058	263	372	1955	23.1
p-xylene	91	126	513	161	223	1271	14.3
o-xylene	91	115	452	150	204	776	13.6
3-ethyltoluene	13	18	93	36	52	651	17
4-ethyltoluene	8	11	51	21	27	322	18
2-ethyltoluene	7	9	36	16	21	181	13
1,3,5-trimethylbenzene	6	10	77	16	29	317	56.7
1,2,4-trimethylbenzene	13	21	160	45	70	955	32.5
1,2,3-trimethylbenzene	4	7	43	15	21	169	32.7
			BVOCs and Its Related Oxidants				
Isoprene	50	51	143	146	141	303	100
α-pinene	6	7	84	14	19	132	52.3
β-pinene	2	3	19	4	4	15	74.3
Limonene	8	32	329	10	21	326	164
Methacrolein (MAC)	39	48	271	61	74	319	29
Methyl vinyl ketone (MVK)	104	135	747	129	148	408	20
			Oxygenated VOCs (OVOCs)				
Formaldehyde	3271	3315	8093	3241	3702	9017	9.4
Acetaldehyde	1107	1243	3921	1452	1774	9096	15
Acetone	3537	3707	8243	3555	3976	9404	0.17
Methanol	3895	4023	10184	4259	4850	16690	0.9
Ethanol	518	670	5576	1271	2809	25209	3.2
n-hexanal	22	36	331	23	34	432	30
			Other VOCs				
$CHCl_3$	72	72	121	97	99	166	0.1
CH_3CCl_3	8	9	11	9	9	28	2.5e-7
CH_2Cl_2	482	551	1410	806	1078	4396	6.1e-7
C_2HCl_3	42	55	190	46	61	263	2.2
C_2Cl_4	64	77	243	99	130	639	0.17
CH_3Cl	1008	1014	1566	1037	1055	1770	7.4e-7
CH_3Br	14	15	42	15	16	40	0.74

Table 1. (continued)

Compound	TMS (pptv)			TW (pptv)			k_{OH}[a]
	Median	Average	Maximum	Median	Average	Maximum	
DMS	3	4	10	5	7	33	5.4
			Non-VOCs				
CO	516	506	660	598	586	858	0.2
NO_2	7	8	29	27	27	62	8.7
CH_4 (ppmv)	2	2	2	2	2	2	6e-3

[a]OH reaction rate coefficients (in 10^{-12} cm^3 molecule^{-1} s^{-1}) at 298 K and 1013 mbar (from *Sander et al.* [2006], *Atkinson and Arey* [2003], *Atkinson et al.* [2006], and the Master Chemical Mechanism, http://mcm.leeds.ac.uk/mcm).

VOC composition (47 ± 2%), followed by alkanes (22 ± 1%), aromatics (12 ± 1%), alkenes (11 ± 1%), other VOCs (i.e., Cl- and Br-contained halocarbons and dimethyl sulfide; 7 ± 0.2%), and BVOCs (1 ± 0.1%). In particular, the most abundant VOC species at TMS were methanol (4023 ± 335 pptv), acetone (3707 ± 334 pptv), formaldehyde (3315 ± 260 pptv), ethane (2015 ± 48 ppbv), toluene (1729 ± 212 pptv), and ethyne (1621 ± 58 pptv). At TW, although OVOCs had the highest contribution to the total VOCs, its percentage was lower than that observed at TMS ($p < 0.05$), with an average value of 38 ± 2%, followed by alkanes (31 ± 2%), alkenes (12 ± 1%), aromatics (12 ± 1%), other VOCs (6 ± 0.5%), and BVOCs (1 ± 0.1%). Methanol (4805 ± 477 pptv), acetone (3976 ± 341 pptv), *n*-butane (3834 ± 540 pptv), formaldehyde (3702 ± 310 pptv), propane (3027 ± 327 pptv), and toluene (2187 ± 558 pptv) were the most abundant VOCs measured at TW. The similar VOC composition at TMS and TW suggested that comparable VOC sources influenced these two sites, reflecting the possible linkage between the mountain site and its foot. Indeed, the earlier studies [*Guo et al.*, 2013; *Lam et al.*, 2013] analyzed mesoscale circulations, i.e., a daytime valley breeze and a nighttime mountain breeze, for the episode days from 27 October to 03 November 2010, inferring that the air mass was carried upslope of TW to TMS during the daytime and switched to a mountain breeze after dusk into the nighttime, with the air mass direction then returning downslope from TMS to TW and that this could influence the redistribution of air pollutants between the two sites.

For NMHCs, although alkanes made the highest contribution, the abundance of individual species was different at the two sites. At TMS, ethane and ethyne were the two major species of NMHCs. These two long-lifetime species, together with relatively higher percentage of OVOCs mentioned above, indicated that the air masses at TMS were aged, which could be transported from the urban centers of Hong Kong and/or the inland PRD region under the influence of mesoscale circulations and regional transport, respectively [*Guo et al.*, 2013; *Lam et al.*, 2013]. On the other hand, the composition of NMHCs at TW was consistent with the findings of an integrated analysis on NMHCs data collected at urban and suburban sites, i.e., Yuen Long, Central/Western, and Tung Chung in Hong Kong, which reported that alkanes were the most important group for ambient NMHCs (44–63%) [*Guo et al.*, 2009; *HKEPD (Hong Kong Protection Department)*, 2010]. Among the alkanes, propane and butanes had relatively higher mixing ratios than other species ($p < 0.05$), suggesting widespread use of liquefied petroleum gas (LPG) in urban areas of Hong Kong, because C_3 and C_4 alkanes are the main component of LPG [*Guo et al.*, 2009, 2011; *Ho et al.*, 2009; *Ling and Guo*, 2014]. In Hong Kong, LPG was being used as fuel for 99.9% of the registered taxis and 51.1% of the public and private light buses by December 2010 [*HKCSD (Hong Kong Census and Statistics Department)*, 2010]. The higher emissions of propane and butanes from LPG usage could be further confirmed by comparing the levels of propane and butanes in this study with those obtained in 2001 at the same TW site. The average values of propane, *n*- and *i*-butane at TW increased from about 2.71, 1.53, and 3.72 ppbv in 2001 [*Guo et al.*, 2004] to about 3.56, 2.83, and 4.27 ppbv in 2010, respectively. Coincidently, the LPG consumption increased from 230,000 t in 2001 to 400,000 t in 2010 in Hong Kong [*HKCSD (Hong Kong Census and Statistics Department)*, 2010].

3.1.2. The OH Reactivity at the Two Sites

In addition to their ambient levels, the OH reactivity of O_3 precursors provides more detailed information on the formation processes of ground level O_3. By investigating the total OH reactivity, the roles of VOCs and NO_x in the balance between perpetuation and termination of O_3 formation reaction sequences could be determined [*Gilman et al.*, 2009; *Mao et al.*, 2010]. Here we compared the total OH reactivity of O_3 precursors

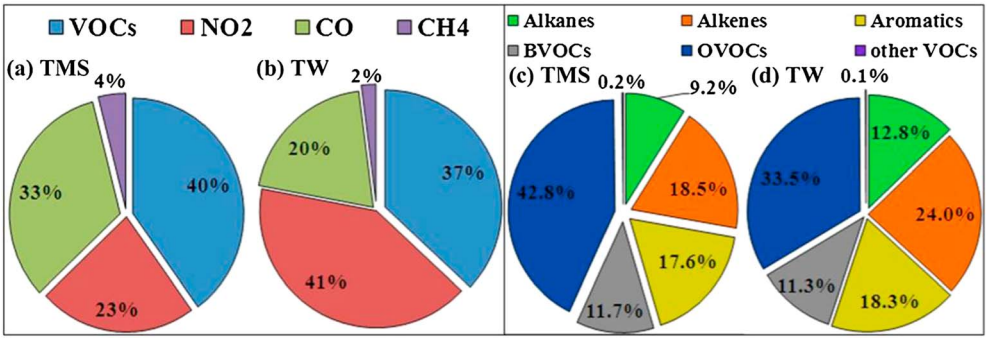

Figure 2. The average contribution of different groups of reactants to the total OH reactivity at TMS and TW. (c and d) The percentage breakdown of (a and b) the constituent VOCs is shown.

in order to better understand the differences of O_3 formation at TMS and TW. The total OH reactivity, i.e., $R_{OH,\ TOTAL}$, the inverse of the OH lifetime, is defined as the sum of the OH reactivity of all the reactants in the atmosphere. It is calculated as the sum of the concentration of each selected reactant multiplied by its reaction rate coefficient with the OH radical, given by equation (1):

$$R_{OH,\ TOTAL} = k_{OH+CH_4}[CH_4] + k_{OH+CO}[CO] + \sum (k_{OH+VOC}[VOC]) + k_{OH+NO_2}[NO_2] = R_{OH,CH_4} + R_{OH,CO} + R_{OH,VOC} + R_{OH,NO_2} \quad (1)$$

The reaction rate coefficients were obtained from the literature [*Sander et al.*, 2006; *Atkinson and Arey*, 2003; *Atkinson et al.*, 2006] and the Master Chemical Mechanism (http://mcm.leeds.ac.uk/mcm). It should be noted that the calculation of OH reactivity in this study only included the measured VOCs, with the measured species accounting for 90% of total carbon at TW and 98% at TMS [*Lam et al.*, 2013]. Undetectable VOCs were excluded, in line with previous studies, which have demonstrated that the measured VOCs give the best available approximation of the ambient OH reactivity [*Di Carlo et al.*, 2004; *Yoshino et al.*, 2006; *Gilman et al.*, 2009], within the limitations of the fieldwork and of the model.

Higher OH reactivity was found at TW. The average values of OH reactivity for VOCs, NO_2, CO, and CH_4 at TW were 5.34 ± 0.38 (average ± 95% confidence interval), 6.08 ± 0.45, 2.91 ± 0.12, and $0.29 \pm 0.01\ s^{-1}$, which are 1.73, 3.44, 1.16, and 1.02 times greater than those measured at TMS, respectively. Figure 2 presents the relative contribution of different constituents to the total OH reactivity at the two sites. At TMS, although VOCs dominated the OH reactivity, the relative percentage contribution of CO was remarkable, which was higher than at TW. This was due to much lower absolute values of the OH reactivity of VOCs and NO_2 at TMS than those at TW. The significant contributions of CO to the total OH reactivity at TMS suggest that CO could react with OH effectively and lead to a significant contribution to O_3 formation, consistent with previous studies conducted in other locations where air masses were aged [*Zhang et al.*, 2008; *Gilman et al.*, 2009]. On the other hand, NO_2 and VOCs had comparable and remarkable contributions to the OH reactivity at TW due to high concentrations of these species, in line with earlier studies undertaken in other urban environments [*Gilman et al.*, 2009; *Mao et al.*, 2010]. Figures 2c and 2d give the contribution of each VOC group to the total OH reactivity of VOCs at the two sites. Among the VOCs, OVOCs were the biggest contributor to the total OH reactivity, followed by aromatics and alkenes at both sites, suggesting the importance of OVOCs in O_3 formation [*Cheng et al.*, 2010]. OVOCs arise from both secondary formation from the oxidation of hydrocarbons and emission from primary sources. The OH reactivity of OVOCs was calculated based on the observation data, which included both the primarily emitted and secondarily formed OVOCs. Hence, the contributions of primary and secondary OVOCs to the total OH reactivity could be different due to the variations of the observed OVOCs at the two sites (Table 1) [*Guo et al.*, 2013]. On the other hand, alkanes and alkenes presented higher contributions to the OH reactivity at TW than at TMS, likely caused by the relatively higher contributions of vehicular emissions to alkanes and alkenes, i.e., propane, *n*/*i*-butanes, ethene, and propene at the urban site [*Ling and Guo*, 2014]. In addition, the contributions of aromatics ($p = 0.60$) and BVOCs ($p = 0.61$) at TMS were comparable to those at TW, and the contributions of other VOCs were negligible at both sites.

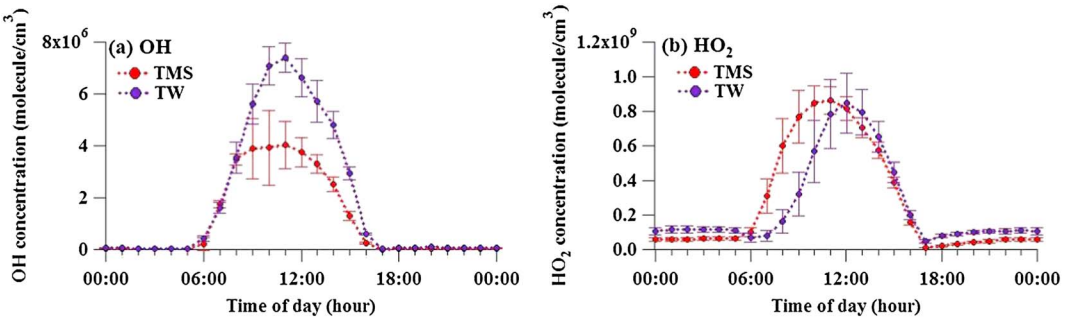

Figure 3. Diurnal variations of (a) OH and (b) HO_2 at TMS and TW.

In summary, the levels and the OH reactivity of O_3 precursors were found to be different at TMS from those at TW. These differences might be the results and/or the causes of differing photochemical reactivity at the two sites. To investigate these differences, in the following section, the photochemical reactivity at the two sites, i.e., the HO_x budget, the OH chain length, the chemical O_3 budget, and the O_3 formation, is explored further using the PBM-MCM.

3.2. Photochemical Reactivity at the Two Sites

3.2.1. The HO_x Budget

Figure 3 shows the diurnal variations of OH and HO_2 simulated by the PBM-MCM at the two sites. As expected, peak values of OH and HO_2 were found around midday at the two sites, consistent with a previous study conducted in the PRD region, in which maximum OH and HO_2 were observed around noon [*Hofzumahaus et al.*, 2009]. The average HO_2 mixing ratio was comparable ($p = 0.05$) at TMS (17.7 ± 2.7 pptv) and TW (14.2 ± 2.3 pptv) during daytime hours (07:00–19:00 LT), with similar peak values of 8.65 and 8.47×10^8 (34.6 and 33.9 pptv) at TMS and TW, respectively. However, the diurnal patterns of HO_2 were different at the two sites. At TMS, the concentrations of HO_2 started to increase at 06:00 LT and reached its maximum value at around noon (11:00 LT), while at TW, the concentrations of HO_2 commenced to enhance with 1 h delay and had a peak value at about 12:00 LT. Furthermore, the mixing ratios of HO_2 in early morning at TW were relatively lower than those at TMS due to the fact that much higher mixing ratios of NO emitted from vehicles at TW consumed more HO_2 through the reaction of $HO_2 + NO$.

On the other hand, the average OH mixing ratio at TW (0.14 ± 0.02 pptv) was higher ($p < 0.05$) by about 1.7 times than at TMS (0.09 ± 0.01 pptv), reflecting the different cycling between OH and HO_2 at the two sites. Note that the calculated OH mixing ratios in this study were slightly different from those previously reported [*Guo et al.*, 2013], because the mixing ratios used here were average values for the period of 27 October to 03 November, while the previous analysis [*Guo et al.*, 2013] used the average mixing ratios for the total 20 non-O_3 and O_3 episode days during the sampling campaign at the two sites. The relatively higher OH mixing ratio at TW was primarily attributed to the higher mixing ratio of NO at this urban site, which shifted the balance of HO_x toward OH by the propagation of HO_2 and RO_2 with NO [*Mao et al.*, 2010]. Since the levels of VOCs were higher at TW, in theory, more RO_2 should be produced accordingly via the reaction of VOCs and OH. However, lower RO_2 mixing ratios were found at the site by model simulation (TW: 9.6 ± 1.3 pptv, TMS: 16.3 ± 2.4 pptv, $p < 0.01$). This is likely due to the fact that there was higher NO mixing ratio at TW and NO reacted with RO_2 to form RO, resulting in more RO_2 being consumed at TW. On the other hand, the RO radical formed could further react with O_2 to form HO_2, which finally generated OH by the reaction with NO. This further confirmed that higher levels of NO shifted the balance of HO_x to OH at TW.

It is of interest to compare the modeled variations of HO_x in this study with the observed data in previous study conducted in inland PRD region [*Hofzumahaus et al.*, 2009]. It was found that although the diurnal patterns of OH and HO_2 at TMS and TW were similar to those observed in inland PRD, the levels of OH and HO_2 during daytime hours were different. The modeled average OH ($2.3–3.6 \times 10^6$ molecules cm^{-3}) and HO_2 concentrations ($3.6–4.4 \times 10^8$ molecules cm^{-3}) were relatively lower in this study than those observed in inland PRD, where the average maximum levels were about 15×10^6 and 18×10^8 molecules cm^{-3} for OH and

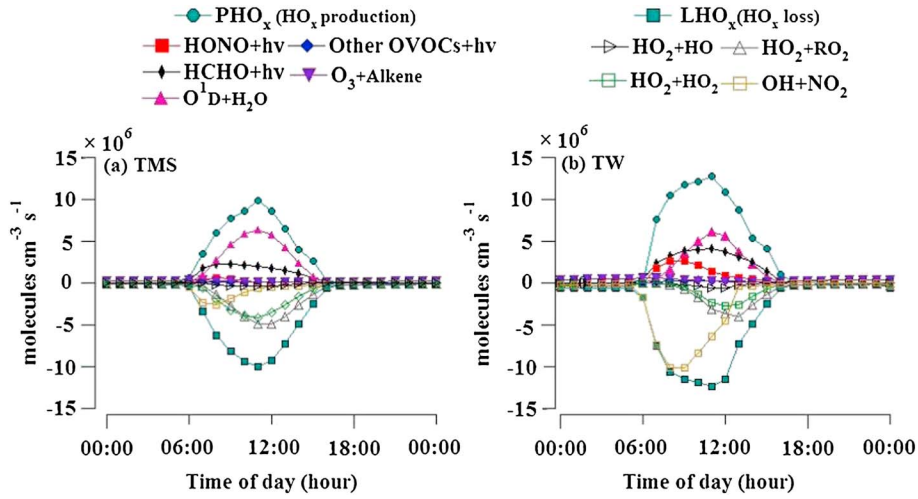

Figure 4. The average diurnal profiles of HO_x sources and sinks at (a) TMS and (b) TW.

HO_2, respectively. The different levels of OH and HO_2 between the two studies could be owing to the differences of measured conditions, i.e., the levels of air pollutants and to a lesser extent, the meteorological conditions, at the different sampling sites [*Hofzumahaus et al.*, 2009; *Lu et al.*, 2012, 2014]. For example, the average mixing ratios of total NMHCs were 11.9 and 23.4 ppbv at TMS and TW, respectively, while the value was about 32 ppbv in the inland PRD region. For individual NMHCs, the average mixing ratios of isoprene were 51 pptv and 141 pptv at TMS and TW, respectively, much lower than that (~1300 pptv) in the inland PRD study. In addition, the average afternoon NO_x level was ~1.2 ppbv in the previous study, while it was about 12.5–48.1 ppbv in this study. On the other hand, by using a generic reaction pathway, i.e., $RO_2 + X \rightarrow HO_2$ and $HO_2 + X \rightarrow OH$ in the Regional Atmospheric Chemical Mechanism model, involving an unidentified compound X and comparing the known OH sources from literatures, it was reported that the high levels of OH in inland PRD might be related to a missing OH source [*Hofzumahaus et al.*, 2009].

To further characterize the photochemical reactivity of HO_x, we investigated the pathway of HO_x sources and sinks at the two sites. The sources of HO_x in this study included the photolysis of O_3 ($O(^1D) + H_2O$), HONO, HCHO, and other OVOCs, peroxides, and the ozonolysis of alkenes, while the HO_x sinks were radical-radical reactions, i.e., $HO_2 + HO_2 \rightarrow HOOH + O_2$, $HO_2 + RO_2 \rightarrow ROOH + O_2$, and $HO_2 + OH \rightarrow H_2O + O_2$, and the reaction between OH and NO_2, i.e., $OH + NO_2 + M \rightarrow HNO_3 + M$. These reactions have been extensively studied in North America and Europe [*Mao et al.*, 2010; *Jenkin and Clemitshaw*, 2000]. Figure 4 illustrates the average diurnal variations of different pathways of HO_x sources and sinks at TMS and TW. Due to the fact that the photolysis of peroxides, i.e., H_2O_2 and CH_3OOH, was minor compared to the reactions shown in Figure 4, they were excluded in the present study [*Sommariva et al.*, 2004; *Jackson and Hewitt*, 1999]. It can be seen that the contributions of pathways to the sources and sinks of HO_x were different at TMS and TW. This is not surprising because the atmospheric constituents were different. During daytime hours, the photolysis of O_3 (with the average contribution of 58%) dominated the HO_x production at TMS, where the O_3 mixing ratios were higher, similar to the results obtained in other rural areas [*Jenkin and Clemitshaw*, 2000; *Ren et al.*, 2008; *Kim et al.*, 2013]. At TW, the major contributors to free radicals were the photolysis of O_3 and HCHO, with the average contributions of 35% and 40% to the total HO_x production, respectively, suggesting that the photolysis of HCHO was an important source of HO_x production, consistent with other studies in urban and suburban environments [*Liu et al.*, 2012; *Mao et al.*, 2010; *Volkamer et al.*, 2010; *Lu et al.*, 2012]. However, this is different from the results reported previously [*Jenkin and Clemitshaw*, 2000; *Mao et al.*, 2010] that determined only the photolysis of HCHO that dominated the HO_x production at urban sites in Europe and Mexico City. The discrepancy was dependent on the differences in HCHO levels in European cities and Mexico City [*Jenkin and Clemitshaw*, 2000; *Shirley et al.*, 2006; *Lei et al.*, 2009]. For instance, although the average O_3 mixing ratio at TW (~40 ppbv) was comparable to that in Europe (~40 ppbv) and slightly lower than in Mexico City (~50 ppbv), the average HCHO mixing ratios were much higher in European cities (~10 ppbv)

and Mexico City (~8.0 ppbv) than those observed at TW (~4.1 ppbv). Nevertheless, the importance of the photolysis of HCHO is consistent in all the studies conducted in urban and suburban environments [*Liu et al.*, 2012; *Volkamer et al.*, 2010]. On the other hand, it is noteworthy that the photolysis of HONO acted as another very important source of HO_x production (with the average contribution of 17% during daytime hours) at TW, especially in the morning rush hour, while its contribution was negligible at TMS. The higher contribution of HONO at TW might be owing to the higher mixing ratios of NO during morning rush hours, resulting in higher levels of HONO through reaction of OH and NO [*Kurtenbach et al.*, 2001; *Li et al.*, 2012]. In fact, the diurnal variations of NO at TW showed a typical urban profile, i.e., bimodal structure, consistent with studies conducted in the urban and suburban areas in Hong Kong [*Guo et al.*, 2009; *Chan et al.*, 1998a]. The first peak was presented in early morning (07:00–09:00 LT), while the second peak appeared at about 18:00–19:00 LT. This observation is in line with the traffic pattern of Hong Kong (Z. Xu et al., Nitrous acid in a polluted subtropical atmosphere: Seasonal variability, direct vehicle emissions, and heterogeneous production at ground level, submitted to *Atmospheric Environment*, 2014). As the reaction of OH and NO is the major pathway for secondary HONO formation, the higher mixing ratios of NO from higher traffic loads in early morning could result in higher mixing ratios of HONO, which would later contribute to the production of OH by photolysis during morning rush hours. Indeed, measurement data indicated that diurnal variation of HONO at the suburban site in Hong Kong presented a peak during morning rush hours (Z. Xu et al., submitted manuscript, 2014). Similar results were also found in some recent urban and suburban studies, in which about 20–35% of HO_x were produced from the photolysis of HONO in urban areas in Berlin, Houston, and Mexico City [*Alicke et al.*, 2003; *Dusanter et al.*, 2009; *Ren et al.*, 2013]. In addition, although the reactions between O_3 and alkenes could produce OH, their contributions were only significant during nighttime hours when HO_x production from photolytic processes was negligible.

At TMS, the radical-radical reactions, i.e., $HO_2 + HO_2$ and $HO_2 + RO_2$, were the major contributors to the HO_x sinks, while the reaction of $OH + NO_2$ was less significant. However, the relative importance of different pathways to HO_x sinks was different at TW, attributable to the differences in ambient conditions [*Jenkin and Clemitshaw*, 2000]. For example, $OH + NO_2$ dominated HO_x sinks at TW in the morning rush hours when the NO_x levels were high [*Guo et al.*, 2013], consistent with the results obtained in a previous study [*Lu et al.*, 2012]. At noon, the radical-radical reactions, i.e., $HO_2 + HO_2$ and $HO_2 + RO_2$, became dominant to the HO_x sinks, with similar rates to those at TMS (~5×10^6 molecules cm^{-3} s^{-1}). The results are consistent with the observations in other urban locations with similar NO_x concentrations, i.e., New York City, Houston, and Mexico City [*Mao et al.*, 2010; *Shirley et al.*, 2006].

3.2.2. Calculated O_3 Production

During daytime hours, in addition to the oxidation of NO to NO_2 by O_3, the most important pathways of converting NO to NO_2 are the oxidation of NO to NO_2 by HO_2 and RO_2 (reactions (2) and (3)) [*Jenkin and Clemitshaw*, 2000].

$$HO_2 + NO \rightarrow OH + NO_2 \quad (2)$$

$$RO_2 + NO \rightarrow RO + NO_2 \quad (3)$$

Due to the fact that the conversion of NO to NO_2 by the above reactions does not consume O_3, the subsequent photolysis of NO_2 (reaction (4)), followed by reaction (5), represents a net source of O_3 [*Jenkin and Clemitshaw*, 2000]:

$$NO_2 + h\nu(\lambda < 420\ \text{nm}) \rightarrow NO + O(^3P) \quad (4)$$

$$O(^3P) + O_2(+M) \rightarrow O_3(+M) \quad (5)$$

Hence, the O_3 production rate was calculated by summing the rates of the reactions between HO_2 and NO and between RO_2 and NO (equation (6)), similar to that described in a previous study using a MCM model [*Xue et al.*, 2013].

$$P(O_3) = k_{HO_2+NO}[HO_2][NO] + \sum k_{RO_{2i}+NO}[RO_{2i}][NO] \quad (6)$$

In addition to its production, O_3 can also be consumed through different mechanisms during daytime hours, i.e., the reactions with HO_2, OH, and unsaturated VOCs, the O_3 photolysis, and reactions that consume NO_x as

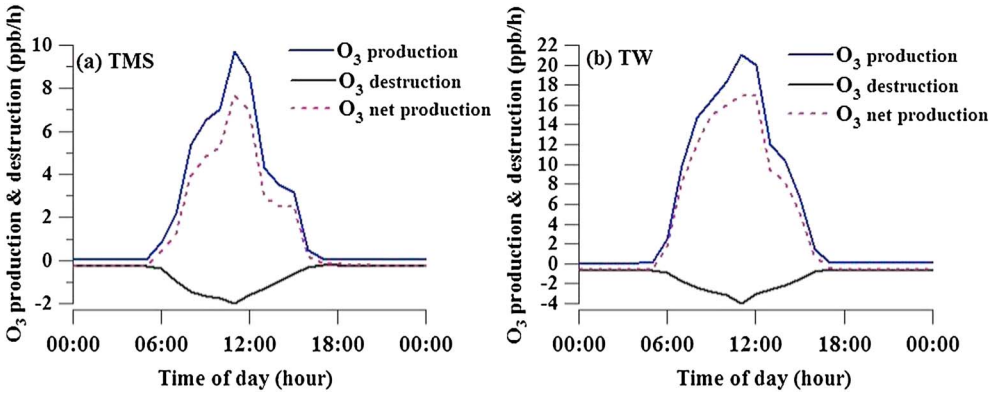

Figure 5. The average diurnal profiles of O_3 production, destruction, and net production at (a) TMS and (b) TW.

described previously [*Ren et al.*, 2013], i.e., the reactions between OH and NO_2 and the formation of $RONO_2$. Thus, the ozone destruction rate can be described as follows (equation (7)):

$$D(O_3) = k_{HO_2+O_3}[HO_2][O_3] + k_{OH+O_3}[OH][O_3] + k_{O(^1D)+H_2O}[O(^1D)][H_2O] + \sum k_{O_3+alkenes}[alkenes][O_3] + k_{OH+NO_2}[OH][NO_2] + P(RONO_2) \quad (7)$$

where the k terms in equations (6) and (7) refer to the reaction rate coefficients of the corresponding reactions. The difference between the O_3 production rate $P(O_3)$ and the O_3 destruction rate $D(O_3)$ represents the net instantaneous O_3 production rate. The O_3 production and destruction rates presented in equations (6) and (7) were calculated based on the modeled species concentration profiles and reaction rate coefficients given in the model and presented as the simulated results. Figure 5 depicts the modeled average diurnal variations of O_3 production, destruction, and net O_3 production rates at TMS and TW. It was found that the O_3 production was significantly greater than the O_3 destruction during daytime hours with peak values at around noon, indicating net O_3 production from in situ photochemistry at the two sites. At TMS, the daytime (07:00–19:00 LT) average net O_3 production rate was estimated to be 2.9 ppb h^{-1}, corresponding to ~36 ppb (i.e., 2.9 ppb $h^{-1} \times 12$ h) O_3 formed from the in situ photochemistry. The amount is coincident with the average increment of O_3 observed from early morning to late afternoon at TMS (~40 ppb), suggesting that in situ photochemical formation significantly contributed to the O_3 increment at TMS, in addition to other factors such as mesoscale circulations and regional transport that shaped the diurnal variations of O_3 [*Guo et al.*, 2013]. On the other hand, the daytime average net O_3 production rate at TW was higher, with a value of 8.1 ppb h^{-1}, indicating that 97 ppb of O_3 could be formed from in situ photochemistry, which was much higher than the observed O_3 increment (~52 ppb). The lower observed O_3 mixing ratios were likely caused by the impact of the in situ emissions of NO_x from nearby emission sources, i.e., vehicular emissions, which titrated part of the O_3 at this urban site [*Hong Kong Transport Department*, 2011; *Lam et al.*, 2013]. As the model results only represent averaged boundary layer values in a well-mixed box [*Lam et al.*, 2013], this effect could not be determined. Analysis of the individual reaction pathways for O_3 production rates found that the reaction between HO_2 and NO dominated the conversion from NO to NO_2 at the two sites, with the average daytime contributions of 63% and 67% at TMS and TW, respectively, while the reactions of $RO_2 + NO$ comprised the remainder, about 37% and 33% to the O_3 production at TMS

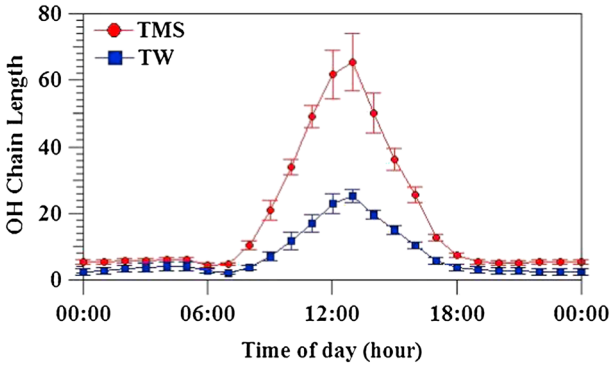

Figure 6. The average diurnal variations of OH chain length at TMS and TW.

and TW, respectively. The results at TW were in agreement with those in New York City and Houston, where the contributions from the reaction between HO_2 and NO to the O_3 production ranged from 54% to 60% [*Ren et al.*, 2003, 2013], and different from that in Nashville, Tennessee, where the contributions to the O_3 production from $HO_2 + NO$ reaction were about the same as that from RO_2 [*Martinez et al.*, 2003]. It should be noted that the O_3 production rates from the reaction of HO_2 and NO (4.8×10^7 molecules cm^{-3} s^{-1}) and from the reaction of RO_2 and NO (2.4×107 molecules cm^{-3} s^{-1}) were much higher at TW ($p < 0.05$), 2.5 and 2.6 times larger, respectively, than those estimated at TMS during daytime hours. Among all the $RO_2 + NO$ reactions, $CH_3O_2 + NO$ had the highest O_3 production rate, with a considerable contribution of 8% and 9% at TMS and TW, respectively. In contrast, the reaction of $OH + NO_2$ was the major mechanism for O_3 destruction at TW, with an average contribution of 41%, while the other reactions composed the remainder. On the other hand, O_3 photolysis and the reaction of $O_3 + HO_2$ were the two major mechanisms for O_3 destruction at TMS, with average contributions of 28% and 34%, respectively, followed by ozonolysis of alkenes (17%), the reactions of $OH + NO_2$ (16%), and $O_3 + OH$ (5%).

3.2.3. The O_3 Production Efficiency

The O_3 production efficiency is closely related to the OH chain length as it is an indicator of HO_x cycling. The OH chain length, defined as the ratio of OH cycling to OH terminal loss, can be calculated using the following equation (equation (8)):

$$\text{OH Chain Length} = \frac{R_{OH} \times [OH] - k_{OH+NO_2+M}[OH] \times [NO_2]}{k_{OH+NO_2+M}[OH] \times [NO_2]} \quad (8)$$

where OH reactivity R_{OH} was calculated in section 3.1.2, $k_{OH+NO2+M}$ was the reaction rate coefficient of NO_2 with OH, while the mixing ratio of OH, i.e., [OH] and the terminal loss of OH by the reaction with NO_2 were from the simulation of PBM-MCM. The longer chain length means that more OH can be regenerated from free radical propagation cycles and subsequently that more O_3 can be produced before termination occurs [*Jenkin and Clemitshaw*, 2000; *Mao et al.*, 2010]. Figure 6 presents the average diurnal variation of OH chain length at TMS and TW. The OH chain length started to increase in the morning and reached its maximum value at noon, consistent with previous studies, in which minimum and maximum values were observed in the morning and at noon, respectively [*Martinez et al.*, 2003; *Emmerson et al.*, 2007; *Mao et al.*, 2010]. The results indicated that the O_3 formation efficiency through the free radical propagation cycles was the highest at noon. The OH chain lengths at TW were between 2 and 25, similar to the results observed in Houston (6–28), but higher than those (3–12) in other U.S. urban cities [*Mao et al.*, 2010]. In contrast, the OH chain lengths at TMS were much higher, with a range of 4–65. This might be caused by the relatively smaller sinks of $OH + NO_2$ due to the lower concentrations of NO_x. Nonetheless, the longer chain length at TMS suggested that the O_3 production was more efficient at TMS than at TW, although the concentrations of precursors and OH and the O_3 production rate were lower.

4. Conclusions

Both similarities and differences of photochemical reactivity at a semirural site and an urban site in Hong Kong were analyzed during an O_3 episode event from October to November in 2010. Much higher O_3 mixing ratios were observed at TMS, while the levels of O_3 precursors, i.e., VOCs and NO_x, were higher at TW. In addition, similar VOC composition at TMS and TW, with the significant contributions of OVOCs and alkanes, indicated the possible linkage between the mountain site and its foot likely through the mesoscale circulations, which influenced the redistribution of air pollutants between the two sites. At TMS, the abundance of long lifetime NMHC species together with relatively higher contributions of OVOCs suggested that the air masses were aged, perhaps related to the air masses transported from the urban centers of Hong Kong and/or the inland PRD region. At TW, the relatively high values of butanes and propane and high contributions of alkanes implied the influence of LPG usage in the urban environments of Hong Kong. The different levels of VOCs and NO_x at TMS and TW resulted in different OH reactivity of O_3 precursors and subsequently different photochemical reactivity at the two sites. Moreover, a PBM-MCM was applied to and constrained by a full suite of measurement data to probe the photochemical reactivity at the two sites, including the HO_x budget, calculated O_3 production rate, and OH chain length. Slightly higher HO_2 concentrations were found at TMS, while much higher OH concentrations were estimated at TW, suggesting that the HO_x cycling processes were different at the two sites, likely caused by the

differences of precursors. The O_3 formation was dominated by the reaction of $HO_2 + NO$ at the two sites. On the other hand, O_3 was mainly destroyed by the reaction of $OH + NO_2$ at TW and by O_3 photolysis and the reaction of $O_3 + HO_2$ at TMS. Furthermore, the OH chain length was used to investigate the O_3 production efficiency with the OH generation at the two sites. A longer OH chain length was found at TMS, indicating that more O_3 could be produced for each radical that was generated at this site.

Acknowledgments

Data supporting Figures 2–6 are available in the supporting information Tables S1–S6. This project is supported by the research grants of the Council of the Hong Kong Special Administrative Region via grants PolyU5179/09E, N_PolyU545/09, and PolyU5154/13E. This study is partly supported by the internal grants of the Hong Kong Polytechnic University (A-PK25 and 1-ZV7A) and the Environment and Conservation Fund (7/2009). We are grateful to Yu Yufan, Choi Yu-Leung, Chan Wai-Lun, Tam Wai Fan, and Shen Yi for their technical support.

References

AFCD (Agriculture, Fisheries and conservation Department) (2008). [Available at http://www.afcd.gov.hk.]

Alicke, B., A. Geyer, A. Hofzumahaus, F. Holland, S. Konrad, H. W. Pätz, J. Schäfer, J. Stutz, A. Volz-Thomas, and U. Platt (2003), OH formation by HONO photolysis during the BERLIOZ experiment, *J. Geophys. Res., 108*(D4), 8247, doi:10.1029/2001JD000579.

Altenstedt, J., and K. Pleijel (2000), An alternative approach to photochemical ozone creation potentials applied under European conditions, *J. Air Waste Manage. Assoc., 50*, 1023–1036.

Atkinson, R., and J. Arey (2003), Atmospheric degradation of volatile organic compounds, *Chem. Rev., 103*, 4605–4658.

Atkinson, R., et al. (2006), Evaluated kinetic and photochemical data for atmospheric chemistry: Volume II – Gas phase reactions of organic species, *Atmos. Chem. Phys., 6*, 3625–4055.

Carslaw, N., D. J. Creasey, D. E. Heard, A. C. Lewis, J. B. McQuaid, M. J. Pilling, P. S. Monks, B. J. Bandy, and S. A. Penkett (1999), Modelling OH, HO_2 and RO_2 radicals in the Marine boundary layer 1: Model construction and comparison with measurements, *J. Geophys. Res., 104*, 30,241–30,255, doi:10.1029/1999JD900783.

Carslaw, N., et al. (2001), OH and HO_2 radical chemistry in a forested region of north-western Greece source, *Atmos. Environ., 35*, 4725–4737.

Chan, L. Y., et al. (1998a), Analysis of the seasonal behavior of tropospheric ozone at Hong Kong, *Atmos. Environ., 32*(2), 159–168.

Chan, L. Y., et al. (1998b), Surface ozone pattern in Hong Kong, *J. Appl. Meteorol., 37*, 1153–1165.

Cheng, H. R., et al. (2010), On the relationship between ozone and its precursors in the Pearl River Delta: Application of an observation-based model (OBM), *Environ. Sci. Pollut. Res., 17*, 547–560.

Derwent, R. G., and T. P. Murrells (2013a), Are photochemical oxidant control strategies robust to the choice of chemical mechanism?, *Environ. Chem., 10*, 234–244.

Derwent, R. G., and T. P. Murrells (2013b), Impact of policy-relevant scenarios on ozone in southern England: Influence of chemical mechanism choice, *Atmos. Environ., 72*, 89–96.

Derwent, R. G., et al. (1998a), Photochemical ozone creation potentials for organic compounds in northwest Europe calculated with a master chemical mechanism, *Atmos. Environ., 32*, 2429–2441.

Derwent, R. G., et al. (1998b), Photochemical ozone creation potentials for organic compounds in northwest Europe calculated with a master chemical mechanism, *Atmos. Environ., 32*, 2429–2441.

Derwent, R. G., et al. (2003), Photochemical ozone formation in northwest Europe and its control, *Atmos. Environ., 37*, 1983–1991.

Derwent, R. G., et al. (2007), Photochemical ozone creation potentials (POCPs) for different emission sources of organic compounds under European conditions estimated with a Master Chemical Mechanism, *Atmos. Environ., 41*, 2570–2579.

Derwent, R. G., et al. (2010), Reactivity scales as comparative tools for chemical mechanisms, *J. Air Waste Manage. Assoc., 60*, 914–924.

Di Carlo, P., et al. (2004), Missing OH reactivity in a forest: Evidence for unknown reactive biogenic VOCs, *Science, 304*, 722–725.

Dusanter, S., et al. (2009), Measurements of OH and HO_2 concentrations during the MCMA-2006 field campaign-Part 2: Model comparison and radical budget, *Atmos. Chem. Phys., 9*, 6655–6675.

Emmerson, K. M., et al. (2005), Urban atmospheric chemistry during the PUMA campaign 1: Comparison of modelled OH and HO_2 concentrations with measurements, *J. Atmos. Chem., 52*, 143–164.

Emmerson, K. M., et al. (2007), Free radical modeling studies during the UK TORCH campaign in summer 2003, *Atmos. Chem. Phys., 7*, 167–181.

Evtyugina, M. G., C. Pio, T. Nunes, P. G. Pinho, and C. S. Costa (2007), Photochemical ozone formation at Portugal West Coast under sea breeze conditions as assessed by master chemical mechanism model, *Atmos. Environ., 41*, 2171–2182.

Gilman, J. B., et al. (2009), Measurements of volatile organic compounds during the 2006 TexAQS/GoMACCS campaign: Industrial influences, regional characteristics, and diurnal dependencies of the OH reactivity, *J. Geophys. Res., 114*, D00F06, doi:10.1029/2008JD011525.

Guo, H., et al. (2004), Source apportionment of ambient non-methane hydrocarbons in Hong Kong: Application of a principal component analysis/absolute principal component scores (PCA/APCS) receptor model, *Envion. Pollut., 129*, 489–498.

Guo, H., et al. (2009), Concurrent observations of air pollutants at two sites in the Pearl River Delta and the implication of regional transport, *Atmos. Chem. Phys., 9*, 7343–7360.

Guo, H., et al. (2011), Which emission sources are responsible for the volatile organic compounds in the atmosphere of Pearl River Delta?, *J. Hazard. Mater., 188*, 116–124.

Guo, H., Z. H. Ling, I. J. Simpson, D. R. Blake, and D. W. Wang (2012), Observations of isoprene, methacrolein (MAC) and methyl vinyl ketone (MVK) at a mountain site in Hong Kong, *J. Geophys. Res., 117*, D19303, doi:10.1029/2012JD017750.

Guo, H., et al. (2013), Characterization of photochemical pollution at different elevations in mountainous areas in Hong Kong, *Atmos. Chem. Phys., 13*, 3881–3898.

Guo, J., et al. (2014), Atmospheric peroxides in a polluted subtropical environment: Seasonal variation, sources and sinks, and importace of heterogeneous processes, *Environ. Sci. Technol., 48*, 1443–1450.

He, Q., C. Li, J. Mao, A. K.-H. Lau, and D. A. Chu (2008), Analysis of aerosol vertical distribution and variability in Hong Kong, *J. Geophys. Res., 113*, D14211, doi:10.1029/2008JD009778.

HKCSD (Hong Kong Census and Statistics Department) (2010), Hong Kong Energy Statistics: Annual Report. [Available at http://www.censtatd.gov.hk.]

HKEPD (Hong Kong Protection Department) (2010), Final report on review on the effectiveness of VOC control programme in Hong Kong. [Available at http://www.epd-asg.gov.hk/english/report/aqr.html.]

HKEPD (Hong Kong Protection Department) (2012a), Integrated Data Analysis and Characterization of Photochemical Ozone in Hong Kong. [Available at http://www.epd-asg.gov.hk/english/report/aqr.html.]

HKEPD (Hong Kong Protection Department) (2012b), Air quality in Hong Kong 2012. [Available at http://www.aqhi.gov.hk/en/download/air-quality-reportse469.html?showall=&start=1.]

HKTD (Hong Kong Transport Department) (2011), The Annual Traffic Census. [Available at http://www.td.gov.hk/filemanager.]
Ho, K. F., et al. (2009), Vehicular emission of volatile organic compounds (VOCs) from a tunnel study in Hong Kong, *Atmos. Chem. Phys.*, *9*, 7491–7504.
Hofzumahaus, A., et al. (2009), Amplified trace gas removal in the troposphere, *Science*, *324*, 1702, doi:10.1126/science.1164566.
Jackson, A. V., and C. N. Hewitt (1999), Atmospheric hydrogen peroxide and organic hydroperoxides: A review, *Crit. Rev. Env. Sci. Technol.*, *29*(2), 175–288.
Jenkin, M. E., and K. C. Clemitshaw (2000), Ozone and other secondary photochemical pollutants: Chemical processes governing their formation in the planetary boundary layer, *Atmos. Environ.*, *34*, 2499–2527.
Jenkin, M. E., et al. (1997a), The tropospheric degradation of volatile organic compounds: A protocol for mechanism development, *Atmos. Environ.*, *31*, 81–104.
Jenkin, M. E. et al. (1997b), Construction and application of a master chemical mechanism (MCM) for modeling tropospheric chemistry, Abstracts of Papers of the American Chemical Society 214, 116-COLL.
Jenkin, M. E., et al. (2003), Protocol for the development of the Master Chemical Mechanism, MCM v3 (Part B): Tropospheric degradation of aromatic volatile organic compounds, *Atmos. Chem. Phys.*, *3*, 181–193.
Jiang, F., et al. (2008), Numerical modeling of a continuous photochemical pollution episode in Hong Kong using WRF-chem, *Atmos. Environ.*, *42*, 8717–8727.
Jiang, F., H. Guo, T. J. Wang, H. R. Cheng, X. M. Wang, I. J. Simpson, A. J. Ding, S. M. Saunders, S. H. M. Lam, and D. R. Blake (2010), An ozone episode in the Pearl River Delta: Field observation and model simulation, *J. Geophys. Res.*, *115*, D22305, doi:10.1029/2009JD013583.
Kim, S., et al. (2013), Evaluation of HO_x sources and cycling using measurement-constrained model calculations in a 2-methyl-3-butene-2-ol (MBO) and monoterpene (MT) dominated ecosystem, *Atmos. Chem. Phys.*, *13*, 2031–2044.
Kurtenbach, R., et al. (2001), Investigations of emissions and heterogeneous formation of HONO in a road traffic tunnel, *Atmos. Environ.*, *35*(20), 3385–3394.
Lam, S. H. M., et al. (2013), Modelling VOC source impacts on high ozone episode days observed at a mountain summit in Hong Kong under the influence of mountain-valley breezes, *Atmos. Environ.*, *81*, 166–176.
Lei, W., et al. (2009), Impact of primary formaldehyde on air pollution in the Mexico City Metropolitan Area, *Atmos. Chem. Phys.*, *9*, 2607–2618.
Li, X., et al. (2012), Exploring the atmospheric chemistry of nitrous acid (HONO) at a rural site in Southern China, *Atmos. Chem. Phys.*, *12*, 1497–1513.
Ling, Z. H., and H. Guo (2014), Contribution of VOC sources to photochemical ozone formation and its control policy implication in Hong Kong, *Environ. Sci. Policy*, *38*, 180–191.
Ling, Z. H., et al. (2011), Source of ambient volatile organic compounds and their contributions to photochemical ozone formation at a site in the Pearl River Delta, southern China, *Environ. Pollut.*, *159*, 2310–2319.
Ling, Z. H., et al. (2013), Establishing a conceptual model for photochemical ozone pollution in subtropical Hong Kong, *Atmos. Environ.*, *76*, 208–220.
Liu, Z., et al. (2012), Summertime photochemistry during CAREBeijing-2007: RO_x budgets and O_3 formation, *Atmos. Chem. Phys.*, *12*, 7737–7752.
Lou, S., et al. (2010), Atmospheric OH reactivities in the Pearl River Delta – China in summer 2006: Measurement and model results, *Atmos. Chem. Phys.*, *12*, 11,243–11,260.
Louie, P. K. K., et al. (2012), VOCs and OVOCs distribution and control policy implications in Pearl River Delta region, China, *Atmos. Environ.*, *76*, 125–135.
Lu, K. D., et al. (2010), Oxidant ($O_3 + NO_2$) production processes and formation regimes in Beijing, *J. Geophys. Res.*, *115*, D07303, doi:10.1029/2009JD012714.
Lu, K. D., et al. (2012), Observation and modelling of OH and HO_2 concentrations in the Pearl River Delta 2006: A missing OH source in a VOC rich atmosphere, *Atmos. Chem. Phys.*, *12*, 1541–1569.
Lu, K. D., et al. (2014), Nighttime observation and chemistry of HOx in the Pearl River Delta and Beijing in summer 2006, *Atmos. Chem. Phys.*, *14*, 4979–4999.
Mao, J. Q., et al. (2010), Atmospheric oxidation capacity in the summer of Houston 2006: Comparison with summer measurements in other metropolitan studies, *Atmos. Environ.*, *44*, 4107–4115.
Martinez, M., et al. (2003), OH and HO_2 concentrations, sources, and loss rates during the Southern Oxidants Study in Nashville, Tennessee, summer 1999, *J. Geophys. Res., 108*(D19), 4617, doi:10.1029/2003JD003551.
NRC (National Research Council) (1991), *Rethinking the Ozone Problem in Urban and Regional Air Pollution*, National Academic Press, Washington, D. C.
Pinho, P. G., et al. (2009), Detailed chemical analysis of regional-scale air pollution in western Portugal using an adapted version of MCM v3.1, *Sci. Total Environ.*, *407*, 2024–2038.
Ren, X. R., et al. (2003), OH and HO_2 chemistry in the urban atmosphere of New York City, *Atmos. Environ.*, *37*, 3639–3651.
Ren, X. R., et al. (2008), HO_x chemistry during INTEX-2004: Observation, model calculation, and comparison with previous studies, *J. Geophys. Res.*, *113*, D05310, doi:10.1029/2007JD009166.
Ren, X. R., et al. (2013), Atmospheric oxidation chemistry and ozone production: Results from SHARP 2009 in Houston, Texas, *J. Geophys. Res. Atmos.*, *118*, 5770–5780, doi:10.1002/jgrd.50342.
Sander, S. P., et al. (2006), Chemical kinetics and photochemical data for use in atmospheric studies, Evaluation Number 15, *JPL Publication*, 10–6.
Saunders, S. M., et al. (2003), Protocol for the development of the Master Chemical Mechanism, MCM v3 (Part A): Tropospheric degradation of non-aromatic volatile organic compounds, *Atmos. Chem. Phys.*, *3*, 161–180.
Seinfeld, J. H., and S. N. Pandis (2006), *Atmospheric Chemistry and Physics: From Air Pollution to Climate Change*, 2nd ed., 1232 pp., Wiley, N. J.
Shirley, T. R., et al. (2006), Atmospheric oxidation in the Mexico City Metropolitan Area (MCMA) during April 2003, *Atmos. Chem. Phys.*, *6*, 2753–2765.
Sillman, S. (1999), The relation between ozone, NO_x and hydrocarbons in urban and polluted rural environments, *Atmos. Environ.*, *33*, 1821–1845.
Simpson, I. J., et al. (2010), Characterization of trace gases measured over Alberta oil sands mining operations: 76 speciated C_2-C_{10} volatile organic compounds (VOCs), CO_2, CH_4, CO, NO, NO_2, NO_y, O_3 and SO_2, *Atmos. Chem. Phys.*, *10*, 11,931–11,954.
Sommariva, R., et al. (2004), OH and HO_2 chemistry in clean marine air during SOAPEX-2, *Atmos. Chem. Phys.*, *4*, 839–856.
Sommariva, R., et al. (2008), A study of organic nitrates formation in an urban plume using a Master Chemical Mechanism, *Atmos. Environ.*, *42*, 5771–5786.

Sommariva, R., et al. (2011), Emissions and photochemistry of oxygenated VOCs in urban plumes in the Northeastern United States, *Atmos. Chem. Phys.*, *11*, 7081–7096.

Utembe, S. R., et al. (2005), Modelling the ambient distribution of organic compounds during the August 2003 ozone episode in the southern UK, *Faraday Discuss.*, *130*, 311–326.

Volkamer, R., et al. (2010), Oxidative capacity of the Mexico City atmosphere-Part 1: A radical source perspective, *Atmos. Chem. Phys.*, *10*, 6969–6991.

Walker, H. L., et al. (2009), Photochemical trajectory modelling of ozone during the summer PUMA campaign in the UK West Midlands, *Sci. Total Environ.*, *407*, 2012–2023.

Wang, T. J., et al. (2006), Integrated studies of a photochemical smog episode in Hong Kong and regional transport in the Pearl River Delta of China, *Tellus Ser. B-Chem. Phys. Meteorol.*, *58*, 31–40.

Wang, T., et al. (2009), Increasing surface ozone concentrations in the background atmosphere of Southern China, 1994-2007, *Atmos. Chem. Phys.*, *9*, 6217–6227.

Xue, L. K., et al. (2013), Sources and photochemistry of volatile organic compounds in the remote atmosphere of western China: Results from the Mt. Waliguan Observatory, *Atmos. Chem. Phys.*, *13*, 8551–8567.

Yang, D. W., C. Li, A. K.-H. Lau, and Y. Li (2013), Long-term measurement of daytime atmospheric mixing layer height over Hong Kong, *J. Geophys. Res. Atmos.*, *118*, 2422–12, doi:10.1022/jgrd.50251.

Yoshino, A., et al. (2006), Measurement of total OH reactivity by laser-induced pump and probe technique – Comprehensive observations in the urban atmosphere of Tokyo, *Atmos. Environ.*, *40*, 7869–7881.

Zhang, J., et al. (2007), Ozone production and hydrocarbon reactivity in Hong Kong, Southern China, *Atmos. Chem. Phys.*, *7*, 557–573.

Zhang, Y. H., et al. (2008), Regional ozone pollution and observation-based approach for analyzing ozone-precursor relationship during the PRIDE-PRD2004 campaign, *Atmos. Environ.*, *42*, 6203–6218.

Zheng, J. Y., et al. (2010), Ground-level ozone in the Pearl River Delta region: Analysis of data from a recently established regional air quality monitoring network, *Atmos. Environ.*, *44*, 814–823.

Zhong, L., et al. (2013), Science-policy interplay: Air quality management in the Pearl River Delta region and Hong Kong, *Atmos. Environ.*, *76*, 3–10.